DESIGN OF NARROW BAND-PASS FREQUENCY SELECTIVE SURFACES FOR MILLIMETER WAVE APPLICATIONS

J.-C. Zhang, Y.-Z. Yin, and J.-P. Ma

National Key Laboratory of Antennas and Microwave Technology
Xidian University
Xi'an, Shaanxi 710071, China

Abstract—A design methodology of narrow band-pass frequency selective surfaces (FSSs) using the Fabry-Perot approach is presented. The whole FSS structure consists of two identical single layer FSSs separated by a foam layer, which forms a Fabry-Perot interferometer (FPI). The band-pass characteristic is a result of the FPI. The pass band can be controlled by the thickness of the foam, and the bandwidth can be controlled by the reflection coefficients of the single layer FSSs. The effects of both metallic and dielectric losses are discussed. It is interesting to note that the transmission peaks of FPI with high Q factor decline rapidly and finally disappear as the losses increase, and the insertion loss is mainly due to the refection. The relationship between the insertion loss and the Q factor of the FPI is examined. As examples, narrow band-pass FSSs at about 96 GHz with different bandwidths are designed.

1. INTRODUCTION

Because of the proceeding occupation of the lower frequency bands and by the growing demand for smaller system dimensions, the millimeter wave region is of increasing importance for wireless communications. Frequency selective surfaces are basically composed of periodic arrays of either conducting patches or apertures from a conducting sheet. In the past four decades, FSSs have found wide applications as spatial filters, absorbers, and polarizers in the microwave, millimeter wave, and infrared community [1–21]. In some applications, narrow band-pass FSSs are required to improve the out-of-band block performance, or to increase the utility and re-use of the available spectrum

---

Corresponding author: J.-C. Zhang (zhang00jch@yahoo.com.cn).

through increased channel selectivity and to reduce adjacent channel leakage. Attempts to the design of narrow band-pass FSSs have been made using aperture coupled microstrip patches [9], or double layer aperture dipole elements, where the response can be controlled by the relative displacement between the arrays [10], or double layer slot rings with different radii [11]. In [12], the Fabry-Perot approach is firstly introduced to design FSSs, and a diagnostic tool is developed. In [13, 14], the Fabry-Parot approach is respectively used to design FSSs with wide transmission band and FSSs for channel demultiplexing. The effects of dielectric losses are also investigated in [14].

However, none of the papers has used Fabry-Parot approach to design a narrow band-pass FSS. Therefore, the aim of this paper is to describe a design methodology of narrow band-pass FSSs using the Fabry-Parot approach. The effects of metallic and dielectric losses on the FPI are carefully investigated. The relationship between the insertion loss and the Q factor of the FPI under different loss levels is examined.

2. ANALYSIS OF FREQUENCY SELECTIVE SURFACES

When a plane wave is incident on the FSS, the total electric field can be decomposed into two parts: the incident field $\vec{E}^i$ due to the incident wave in the absence of the metallic layer, and the scattered field $\vec{E}^s$, which is the result of the electric current $\vec{J}$ induced on the metallic layer. The metallic layer is assumed to be infinitely thin. The relation between the transverse components of $\vec{E}^s$ and $\vec{J}$ in the spectral domain can be written as [1–3]

$$
\begin{cases}
\tilde{E}^s_x = \tilde{G}_{xx}\tilde{J}_x + \tilde{G}_{xy}\tilde{J}_y \\
\tilde{E}^s_y = \tilde{G}_{yx}\tilde{J}_x + \tilde{G}_{yy}\tilde{J}_y
\end{cases}
\tag{1}
$$

where $\tilde{G}_{xx}$, $\tilde{G}_{xy}$, $\tilde{G}_{yx}$, $\tilde{G}_{yy}$ are the components of the dyadic Green's function. The script '∼' denotes the Fourier transformation, which is defined as

$$
\tilde{f}(\alpha, \beta) = \int\limits_{-\infty}^{+\infty} \int\limits_{-\infty}^{+\infty} f(x, y)e^{-j(\alpha x + \beta y)}dxdy
\tag{2}
$$

Applying the boundary condition at the metallic layer, that is, $\vec{E}^i + \vec{E}^s = R_s\vec{J}$ at the conducting area, where R_s is the resistance of the conductor, and considering the periodic property of the FSS, the

well known electric field integral equation (EFIE) of the FSS is given as [1–3]

$$\begin{cases} -E_x^i = \frac{1}{T_x T_y} \sum_{m,n=-\infty}^{+\infty} \left(\tilde{G}_{xx} \tilde{J}_x + \tilde{G}_{xy} \tilde{J}_y \right) e^{j(\alpha_m x + \beta_n y)} \\ -E_y^i = \frac{1}{T_x T_y} \sum_{m,n=-\infty}^{+\infty} \left(\tilde{G}_{yx} \tilde{J}_x + \tilde{G}_{yy} \tilde{J}_y \right) e^{j(\alpha_m x + \beta_n y)} \end{cases} \tag{3}$$

where T_x, T_y are the periodicities, and

$$\alpha_m = \frac{2\pi m}{T_x} + k_0 \sin\theta \cos\varphi, \quad \beta_n = \frac{2\pi n}{T_y} + k_0 \sin\theta \sin\varphi \tag{4}$$

with k_0 is the wave number of free space, and θ, φ are the elevation and azimuth angles of incidence, respectively.

The incident electric field and the Green's function can be calculated by the spectral immitance approach. The EFIE is solved by the Galekin's moment method (MM), and the rooftop basis function is used to expand the electric current. After the electric current is solved, the fields at each interface are ready to know, and consequently the reflection and transmission coefficients.

The cascading technique of the scattering matrix is used to calculate the frequency response of multilayer FSSs, which is given as [1–3]

$$S_{11}^c = S_{11}^1 + S_{12}^1 R S_{11}^2 S_{21}^1$$
$$S_{12}^c = S_{12}^1 R S_{12}^2$$
$$S_{21}^c = S_{21}^2 T S_{21}^1$$
$$S_{22}^c = S_{22}^2 + S_{21}^2 T S_{22}^1 S_{12}^2$$

where $R = [\mathbf{I} - S_{11}^2 S_{22}^1]^{-1}$, $T = [\mathbf{I} - S_{22}^2 S_{11}^1]^{-1}$, and $\mathbf{I}$ is the identity matrix. The superscripts 1, 2, c of S denote network 1, network 2, and the composite network, as shown in Fig. 1.
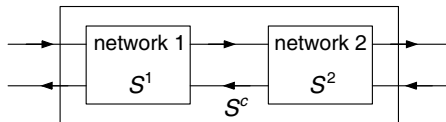

Figure 1. Cascading of two networks.

3. THE DOUBLE LAYER FSS FABRY-PEROT INTERFEROMETER

As shown in Fig. 2, the FPI consists of a double layer FSS structure. The single layer FSS is composed of a metallic layer (periodic array)
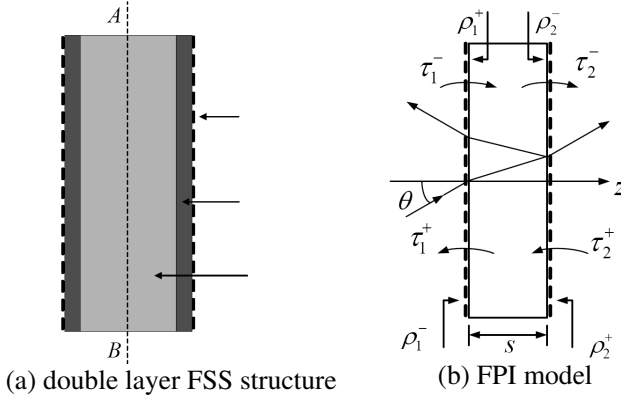
(a) double layer FSS structure   (b) FPI model

Figure 2. Double layer FSS structure and its FPI model [12].

and a dielectric substrate. It should be noted that the single layer FSS is regarded as a single structure, which is equivalent to the interface (a network) of the FPI. The reflection and transmission coefficients on either side of the foam (scattering parameters) can be written as [12]

$$\rho_i^{-(+)} = R_i^{-(+)} e^{j\phi_i^{-(+)}} \tag{5}$$

$$\tau_i^{-(+)} = T_i^{-(+)} e^{j\vartheta_i^{-(+)}} \tag{6}$$

where $R_i^{-(+)}$, $T_i^{-(+)}$ are the magnitudes, and $\phi_i^{-(+)}$, $\vartheta_i^{-(+)}$ the phases, with i denoting the left and right side and $-(+)$ the coefficients of incident waves traveling from $-(+)z$. $\rho_1^{-(+)}$, $\tau_1^{-(+)}$ are obtained by solving a single layer FSS with the left side semi infinite air and the right side semi infinite foam. Similarly, $\rho_2^{-(+)}$, $\tau_2^{-(+)}$ are obtained by solving a single layer FSS with the left side semi infinite foam and the right side semi infinite air.

According to the cascading technique of the scattering matrix, after some algebraic manipulations the reflection and transmission coefficients of the FPI can be written respectively as

$$S_{11} = \rho_1^- + \frac{\tau_1^- \tau_1^+}{1 - \rho_1^+ \rho_2^- e^{-j2\beta s}} \rho_2^- e^{-j2\beta s} \tag{7}$$

and

$$S_{21} = \frac{\tau_1^- \tau_2^-}{1 - \rho_1^+ \rho_2^- e^{-j2\beta s}} \tag{8}$$

where

$$\beta = \frac{2\pi}{\lambda_0} \sqrt{\varepsilon_r - \sin^2 \theta} \tag{9}$$

and ε_r, s are the dielectric constant and the thickness of the foam, respectively, and λ_0 is the wavelength in the free space.

From (8), we can obtain

$$|S_{21}|^2 = \frac{(T_1^- T_2^-)^2}{1 - 2R_1^+ R_2^- \cos \Phi + (R_1^+ R_2^-)^2} \tag{10}$$

where

$$\Phi = 2\beta s - \phi_1^+ - \phi_2^- \tag{11}$$

According to the energy conservation law, yield

$$\left(R_{1(2)}^{+(-)} \right)^2 + \frac{\eta_0}{\eta} \left(T_{1(2)}^{+(-)} \right)^2 + L_{1(2)}^{+(-)} = 1 \tag{12}$$

$$\left(R_{1(2)}^{-(+)} \right)^2 + \frac{\eta}{\eta_0} \left(T_{1(2)}^{-(+)} \right)^2 + L_{1(2)}^{-(+)} = 1 \tag{13}$$

where L terms denote the normalized dissipated power of the interfaces, η_0, η are the wave admittance of free space and the foam, respectively.

According to the reciprocal theory, yield

$$\left(T_{1(2)}^{-(+)} \right)^2 = \left(\frac{\eta_0}{\eta} \right)^2 \left(T_{1(2)}^{+(-)} \right)^2 \tag{14}$$

As the FPI is symmetrical, $R_1^+ = R_2^- = R$, $T_1^+ = T_2^- = T$, $L_1^+ = L_2^- = L$. Therefore, (8), (10) and (12) can be rewritten respectively as

$$S_{11} = \rho_1^- + S_{21} \rho_2^- e^{-j2\beta s} \tag{15}$$

$$|S_{21}|^2 = \left(\frac{\eta_0}{\eta} \right)^2 \frac{T^4}{1 - 2R^2 \cos \Phi + R^4} \tag{16}$$

$$R^2 + \frac{\eta_0}{\eta} T^2 + L = 1 \tag{17}$$

Obviously, $|S_{21}|$ is maximum when $\cos \Phi = 1$, which means

$$\frac{2\pi s}{\lambda_0} \sqrt{\varepsilon_r - \sin^2 \theta} - n\pi = \frac{\phi_1^+ + \phi_2^-}{2} = \phi, \quad n = 0, 1, 2, \cdots \tag{18}$$

In this case, considering (17), (16) can be rewritten as

$$|S_{21}|^2 = \left(\frac{\eta_0}{\eta} \right)^2 \frac{T^4}{\left(\frac{\eta_0}{\eta} T^2 + L \right)^2} \tag{19}$$

The Q factor is defined as

$$Q = \frac{4R}{(1 - R)^2} \tag{20}$$

4. DESIGN OF NARROW BAND-PASS FSSS

First, let the single layer FSS resonates (maximum reflection) at the wanted frequency by changing the dimensions of the elements. In this step, the conducting and dielectric losses can be neglected. It should be noted that the incident wave is from the semi infinite foam. Second, let the FPI resonates (transmission peak) at the wanted frequency by changing the thickness of the foam s. An initial vale of s can be obtained by the following equation:

$$s = \frac{(\phi + n\pi)\lambda_0}{2\pi\sqrt{\varepsilon_r - \sin^2\theta}} \qquad (21)$$

The bandwidth obtained in this way, where the resonant frequency of the single layer FSS is consistent with that of the FPI, can be extremely narrow. The bandwidth will be broader as the resonant frequency of the single layer FSS departs from that of the FPI. In other words, the bandwidth can be controlled by the reflection coefficient of the single layer FSS.

5. NUMERICAL RESULTS AND DISCUSSION

To validate the MM analysis of the FSS, Fig. 3 compares the results obtained in this work and those presented by Lima in [12]. The results were obtained for a square loop FSS (see Fig. 4) on a dielectric substrate with thickness 0.323 mm and dielectric constant 3.78. Our results are in a good agreement with those shown in [12].

Next, design of narrow band-pass FSSs using the FPI, which consists of a symmetrical double layer FSS structure, is demonstrated.
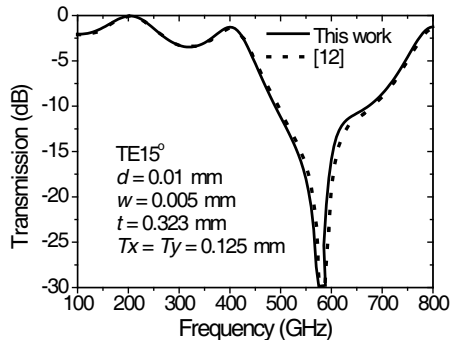

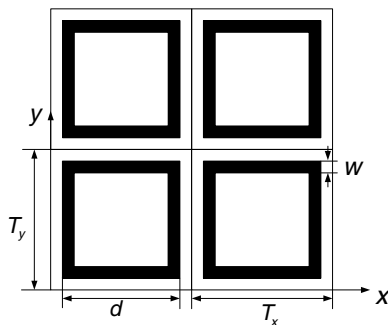**Figure 3.** Comparison between the results obtained in this work and those presented in [12].

Figure 4. A square loop FSS and its dimensions.
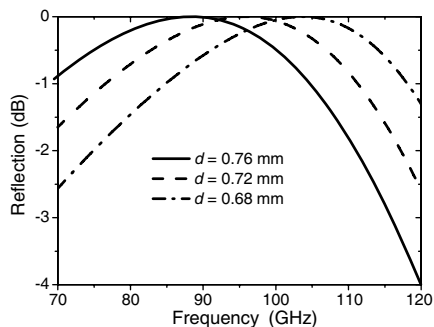

Figure 5. Reflection coefficients of the single layer FSS.

As shown in Fig. 2, the thickness of the dielectric layer is 0.127 mm, and the dielectric constant 3.78. The dielectric constant of the foam is 1.1. Fig. 5 shows the reflection coefficients of the single layer FSS versus frequency for different d with $w = 0.06$ mm and $T_x = T_y = 1$ mm. It can be seen that when $d = 0.72$ mm, the element resonates at about 96 GHz. As demonstrated above, narrowest bandwidth will be obtained at $d = 0.72$ mm. The phase of the reflection coefficient in this case is $147.1°$ at $f = 96$ GHz. From (21), yield

$$s = 1.2175 \,\text{mm}, \ n = 0$$
$$s = 2.7073 \,\text{mm}, \ n = 1$$

Figure 6 shows the phase term of either side of (18) with different s. Note that for each s, considering the periodicity 2π from (16), the variable n in the left side of (18) may have two values: 0 and 1. Therefore, each s corresponds two diagonal lines, which have a difference of $180°$ (or $-180°$). It is clear that the slope of the lines for $s = 1.2175$ mm is much less than that for $s = 2.7073$ mm. The three curves intersect at about $f = 96$ GHz. Hence, a transmission peak at about 96 GHz will appear. There are two other points of intersection for $s = 2.7073$ mm, and one for $s = 1.2175$ mm in the frequency range from 50 GHz to 150 GHz, respectively. These points of intersection mean extra transmission peaks.

Figure 7 shows the reflection coefficients of the FPI (double layer FSS structure) for both s. The resonant frequencies occur at 96.0092 GHz, 95.9825 GHz, with -10 dB bandwidth 0.00033 GHz, 0.00012 GHz, respectively. The resonant frequencies are either slightly smaller or greater than the expected, 96 GHz, which may be due to the coupling of the two screen. This can be adjusted by slightly changing s. For example, the resonant frequency increases from 95.9825 GHz to

96.0018 GHz by changing $s = 2.7073$ mm to $s = 2.7064$ mm. However, exactly 96 GHz may need many numbers after the radix point, because the resonant frequency is very sensitive to s.

Figure 8 shows the transmission coefficients of the FPI in a wider frequency band. As expected, extra transmission peaks occur at 139 GHz for $s = 1.2175$ mm and 60.5 GHz, 126 GHz for $s = 2.7073$ mm, respectively. On other words, in a wide range from 50 GHz to 139 GHz for $s = 1.2175$ mm or from 60.5 GHz to 126 GHz for $s = 2.7073$ mm, there is only one transmission peak. It can be seen that for $s = 1.2175$ mm the FPI has better out-of-band performance while for $s = 2.7073$ mm the FPI has a narrower bandwidth. The FPI is assumed to be lossless in Figs. 5–8.
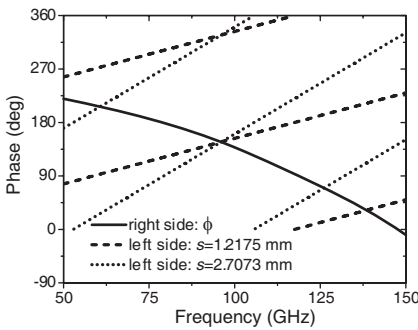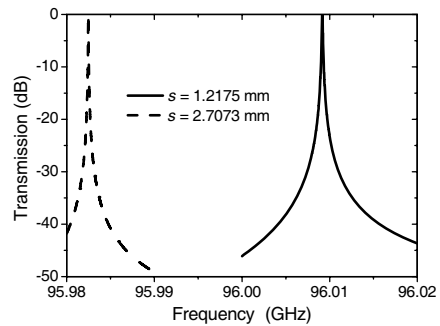

Figure 6. Phase diagram for the FPI.

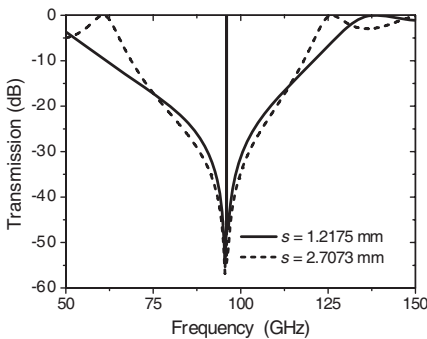**Figure 7.** Transmission coefficients of the FPI.

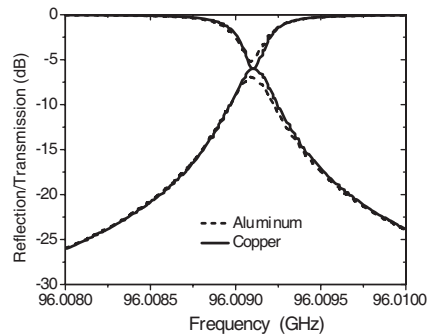**Figure 8.** Transmission coefficients of a high Q FPI in a wider frequency band.

Figure 9. Frequency response of a high Q FPI for the aluminum and copper conductors.

Figure 9 shows the frequency response of the FPI for the aluminum and copper conductors rather than the perfect conductor. The transmission peaks decline significantly with insertion loss $-6.935\,\text{dB}$ and $-6.008\,\text{dB}$, respectively. The dissipated power is $-3.054\,\text{dB}$ and $-3.134\,\text{dB}$, respectively. The result shows that both the dissipated and reflected powers for the aluminum are greater than that for the copper due to its smaller conductance.

Figure 10 shows the reflection and transmission coefficients of the FPI for different dielectric loss tangents. It can be seen that the transmission peak declines rapidly and finally disappears as the loss tangent increases. It is interesting to note that for a high Q FPI, as the transmission peak disappears, the insertion loss is mainly due to the refection rather than the dissipation. This may be very useful for broadband band-stop FSSs, for example, the FSS for $s = 1.2175\,\text{mm}$ will have a stop bandwidth of $65.5\,\text{GHz}$ if the center transmission peak is suppressed. (15) and (19) will give a good interpretation for the disappearance of the transmission peak and the reflection of the power:

If $T^2 \ll L$, from (19), $|S_{21}| \to 0$, this suggests the disappearance of the transmission peak.

If $|S_{21}| \to 0$, from (15), $S_{11} \to \rho^-$, this means that the reflection coefficient of the FPI is close to that of the single layer FSS. If L is small, which is true for most conductors and dielectrics, most of the power will be reflected. Consider the FPI in Fig. 10 with $\tan\delta = 1.0e{-}3$ at $f = 96.0092\,\text{GHz}$ as an example, the transmission coefficient of the single layer FSS is $T^2 = 8.22e - 06$, while the dielectric loss is $6.24e - 04$. From (19), $S_{21} = 1.36e - 2$ or $-37.33\,\text{dB}$. The transmission and reflection coefficients of the FPI in Fig. 10 obtained from MM are $-38.15\,\text{dB}$, $-0.108\,\text{dB}$, respectively. Note that in Figs. 9 and 10 the dielectric loss and the conductor loss are discussed separately, that is,
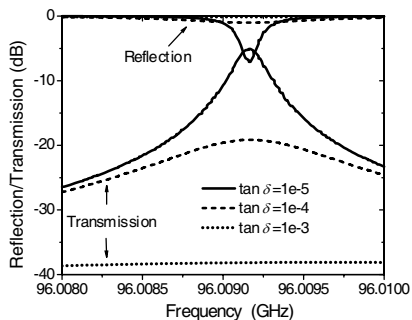

Figure 10. Frequency response of a high Q FPI for different dielectric loss tangents.
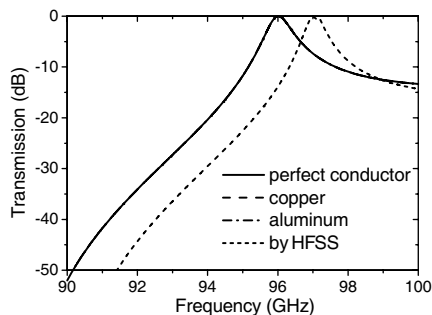
Figure 11. Transmission coefficient of the low Q FPI for different conductors.

it is assumed that there is no dielectric loss when considering conductor losses, and vice versa. The foam is assumed to be lossless.

As mentioned in Section 4, broader bandwidth can be obtained from shifting the resonance of the single layer away from that of the FPI. The shifting can be realized by changing the element dimensions. Comparisons of transmission coefficients of the FPI for different conductors and dielectrics with different loss tangents are respectively shown in Figs. 11 and 12 with $d = 0.76$ mm and $w = 0.06$ mm. The thickness of the foam is obtained from (18) with the result $s = 1.1047$ mm. As shown in Fig. 11, the resonant frequency obtained is 96.0150 GHz, with -10 dB bandwidth 2.50 GHz, about 2.6%. It can be observed that there is little distinction among the frequency response of FPI with the aluminum, copper and the perfect conductor, the transmission curves almost coincide with each other. Fig. 11 also shows the simulated results by HFSS. As can be seen, the resonant frequency simulated by HFSS is about 97 GHz, slightly larger than that obtained from the MM. Except this difference, good agreement is observed. Compared with lossless dielectrics, Fig. 12 shows that the transmission coefficient declines distinctly at $\tan\delta = 1.0e - 2$ but has little change at $\tan\delta = 1.0e - 3$, which is commercially available. It should be noted that the insertion loss in this case is mainly due to the absorption, not the reflection. It is undesired that in the upper band the transmission coefficient declines slowly, which is due to the lower Q factor.

Figure 13 shows the transmission coefficients of the FPI versus Q factor for different L. As can be seen, for low Q factor, the insertion loss is mainly due to the dissipation, which is about $2L/T$ if L is much smaller than T. As the Q factor increases, the transmission coefficient decreases rapidly, and finally goes to zero.
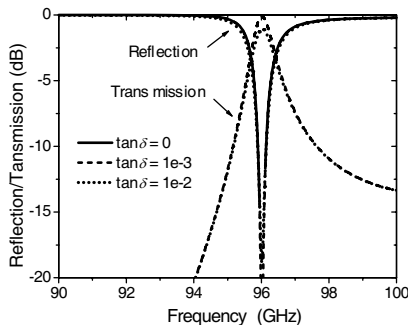

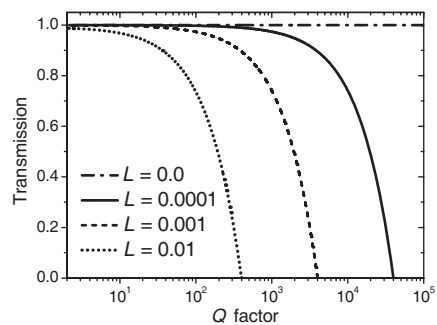**Figure 12.** Frequency response of the low Q FPI for different dielectric loss tangents.

Figure 13. Frequency response of the FPI for different loss levels.

6. CONCLUSION

A design methodology of narrow band-pass FSSs using the Fabry-Perot approach is developed. The resonant frequency is controlled by the thickness of the foam, while the bandwidth is determined by the reflection coefficient of the FPI interface. The effects of the metallic and dielectric losses are investigated. The results show that for a high Q FPI the transmission peak declines rapidly and finally disappears as the losses tangent increases. It is interesting that as the transmission peak disappears, most of the power is not dissipated but reflected. It should be noted that the resonant frequency is very sensitive to the thickness and will change if the angle of incidence changes.

REFERENCES

1. Vacchione, J. D., "Techniques for analysing planar, periodic, frequency selective surface systems," Ph.D. Dissertation, Dept. Elect. Eng., Univ. of Illinois at Urbana-Champaign, 1990.

2. Mittra, R., C. H. Chan, and T. Cwik, "Techniques for analyzing frequency selective surfaces — A review," *IEEE Proceedings*, Vol. 76, 1593–1615, 1988.

3. Wan, C. and J. A. Encinar, "Efficient computation of generalized scattering matrix for analyzing multilayered periodic structures," *IEEE Trans. Antennas Propagat.*, Vol. 43, 1233–1242, 1995.

4. Fadi, S., N.-O. Yair, R. Amichai, et al., "Absorbing frequency-selective-surface for the mm-wave range," *IEEE Trans. Antennas Propagat.*, Vol. 56, 2649–2655, 2008.

5. Sha, Y.-N., K. A. Jose, C. P. Neo, et al., "Experimental investigations of microwave absorber with FSS embedded in carbon fiber composite," *Microw. Opt. Tech. Lett.*, Vol. 32, 245–249, 2002.

6. Euler, M. and V. Fusco, "Sub-millimetre wave linear to circular polariser converter," *Loughborough Antennas & Propagation Conference*, 77–80, Loughborough, UK, 2008.

7. Yoshihisa, I. and T. Takano, "Frequency selective surfaces for radio astronomy," *Experimental Astronomy*, Vol. 2, 123–136, 1991.

8. Shelton, D. J., J. W. Cleary, et al., "Gangbuster frequency selective surface metamaterials in terahertz band," *Electronics Letters*, Vol. 44, 1288–1289, 2008.

9. Pozar, D. M. and R. Pous, "A frequency selective surface using aperture coupled microstrip patches," *Antennas and Propagation Society International Symposium*, Vol. 1, 96–99, 1990.

10. Lockyer, D. S. and J. C. Vardaxoglou, "Reconfigurable FSS response from two layers of slotted dipole arrays," *Electronics Letters*, Vol. 32, 512–513, 1996.

11. Parker, E. A. and A. Stanley, "Dual-polarized narrow-bandpass frequency-selective surfaces," *Microw. Opt. Tech. Lett.*, Vol. 13, 105–107, 1996.

12. De Lima, A. C. C. and E. A. Parker, "Fabry-perot approach to the design of double layer FSS," *IEE Proc. - Microw. Antennas Propag.*, Vol. 143, 157–162, 1996.

13. Antonopoulos, C. and E. A. Parker, "Design procedure for FSS with wide transmission band and rapid rolloff," *IEE Proc. - Microw. Antennas Propag.*, Vol. 145, 508–510, 1998.

14. Cahill, R., I. M. Sturland, J. W. Bowen, et al., "Frequency selective surfaces for millimetre and submillimetre wave quasi optical demultiplexing," *Int. J. of Infrared and Millimeter Waves*, Vol. 14, 1769–1788, 1993.

15. Ma, D. and W. S. Zhang, "Mechanically tunable frequency selective surface with square-loop-slot elements," *Journal of Electromagnetic Waves and Applications*, Vol. 21, No. 15, 2267–2276, 2007.

16. Guo, C., H. Sun, and X. Lu,, "A novel dualband frequency selective surface with periodic cell perturbation," *Progress In Electromagnetics Research B*, Vol. 9, 137–149, 2008.

17. Ucar, M. H. B., A. Sondas, and Y. E. Erdemli, "Switchable split-ring frequency selective surfaces," *Progress In Electromagnetics Research B*, Vol. 6, 65–79, 2008.

18. Zhang, J. C., Y. Z. Yin, and J. P. Ma, "Frequency selective surfaces with fractal four legged elements," *Progress In Electromagnetics Research L*, Vol. 8, 1–8, 2009.

19. Oraizi, H. and M. Afsahi, "Design of metamaterial multilayer structures as frequency selective surfaces," *Progress In Electromagnetics Research C*, Vol. 6, 115–126, 2009.

20. Farahat, A. E. and K. F. A. Hussein, "Spatial filters for linearly polarized antennas using free standing frequency selective surface," *Progress In Electromagnetics Research M*, Vol. 2, 167–188, 2008.

21. Zhuang, W., Z. H. Fan, D. Z. Ding, et al., "Fast analysis and design of frequency selective surface using the GMRESR-FFT method," *Progress In Electromagnetics Research B*, Vol. 12, 63–80, 2009.